Ultrasound in Med. & Biol., Vol. 31, No. 9, pp. 1245–1256, 2005

0301-5629/05/$–see front matter

ELSEVIER

doi:10.1016/j.ultrasmedbio.2005.02.017

● *Original Contribution*

CAVITATION DETECTION DURING SHOCK-WAVE LITHOTRIPSY

MICHAEL R. BAILEY,* YURI A. PISHCHALNIKOV,† OLEG A. SAPOZHNIKOV,‡
ROBIN O. CLEVELAND,§ JAMES A. MCATEER,† NATHAN A. MILLER,*
IRINA V. PISHCHALNIKOVA,† BRET A. CONNORS,§ LAWRENCE A. CRUM,* and
ANDREW P. EVAN†

*Center for Industrial and Medical Ultrasound, Applied Physics Laboratory, University of Washington, Seattle, WA, USA; †Department of Anatomy and Cell Biology, Indiana University School of Medicine, Indianapolis, IN, USA; ‡Department of Acoustics, Faculty of Physics, M.V. Lomonosov Moscow State University, Moscow, Russia; and §Department of Aerospace and Mechanical Engineering, Boston University, Boston, MA, USA

(*Received* 7 *October* 2004, *revised* 17 *February* 2005, *in final form* 25 *February* 2005)

Abstract—A system was built to detect cavitation in pig kidney during shock-wave lithotripsy (SWL) with a Dornier HM3 lithotripter. Active detection using echo on B-mode ultrasound, and passive cavitation detection using coincident signals on confocal orthogonal receivers, were used to interrogate the renal collecting system (urine) and the kidney parenchyma (tissue). Cavitation was detected in urine immediately upon shock-wave (SW) administration in urine or urine plus X-ray contrast agent but, in native tissue, cavitation required hundreds of SWs to initiate. Localization of cavitation was confirmed by fluoroscopy, sonography and by thermally marking the kidney using the passive cavitation detection receivers as high-intensity focused ultrasound sources. Cavitation collapse times in tissue and native urine were about the same, but less than in urine after injection of X-ray contrast agent. The finding that cavitation occurs in kidney tissue is a critical step toward determining the mechanisms of tissue injury in SWL. (E-mail: bailey@apl.washington.edu) © **2005 World Federation for Ultrasound in Medicine & Biology.**

Key Words: **Cavitation, Lithotripsy, Shock wave, Ultrasound.**

INTRODUCTION

Studies (Delius et al. 1990; Evan et al. 2002; Zhu et al. 2004) designed to enhance or suppress cavitation show a corresponding tissue injury response and provide indirect evidence that cavitation contributes to tissue damage during shock-wave lithotripsy (SWL). Both B-mode ultrasound (US) (Delius and Gambihler 1992; Kuwahara et al. 1989) and focused, single-element, passive receivers (Coleman et al. 1996; Zhong et al. 1997) have been used separately in attempts to establish direct evidence of cavitation within the kidney. However, when only one transducer has been used, it has not been possible to discem if cavitation actually occurs within kidney parenchyma, as opposed to the fluid spaces of the collecting system (Cleveland et al. 2000b).

The *in vivo* cavitation detection system described here uses dual confocal passive transducers to sample a small volume and B-mode US to give visual localization of the site of acoustic emissions. This system allows for precise targeting and confirmation of cavitation signals within specific anatomical regions of the kidney. We describe in detail the components of the system and alignment of the transducers, demonstrate the ability of the system to target selectively renal tissue or the urine collecting system of the kidney and describe the observed evolution of cavitation during SWL.

Address correspondence to: Michael R. Bailey, Applied Physics Laboratory, University of Washington, 1013 NE 40th St., Seattle, WA 98105 USA. bailey@apl.washington.edu

MATERIALS AND METHODS

Lithotripter

Experiments were conducted using an unmodified (80 nF capacitor) Dornier HM3 electrohydraulic lithotripter (Dornier GmbH, Germany) at charging voltages of predominantly 18 and 24 kV, but also 15 and 21 kV. The Dornier HM3 is a bathstyle lithotripter in which the patient is immersed in water and there is no barrier between the shock source and the patient. Refurbished

electrodes (Service Trends, Kennesaw, GA, USA) were used after conditioning with 150 shock waves and were discarded after 2000 shock waves.

Animal model

Three normal 6-week-old pigs were used. Animal preparation, anesthetization, surgery, lithotripsy treatment and euthanasia followed an established institutionally approved protocol (Evan et al. 1998) that complied with legal requirements and institutional guidelines. Balloon catheters were surgically inserted in both ureters of the anesthetized pig. The midline abdominal incision was closed with effort to minimize trapping of air by keeping the animal supine and compressing the abdomen by hand. The catheter permitted the injection of X-ray contrast agent into the urine collecting system. The back and sides of the pig were carefully shaved by razor. Any remaining hair was removed by a depilation agent such as Nair (Church & Dwight Co., Princeton, NY, USA).

Several steps were taken to prepare the animals for cavitation detection. A B-mode US scanner (SonoSite 180, C15/4-2 scan head) was used to examine acoustic windows for access of passive cavitation detection (PCD) and US examination and to assess for air pockets that might have been introduced during insertion and positioning of the ureteral catheters. In no case was air found trapped within the animal. Location of the ribs was marked on the skin to aid in positioning the transducers. Also, after the animal was in final position for SW treatment, the skin was massaged to release bubbles and particles from the skin.

The right kidney was treated, removed and fixed according to our previously published method (Evan et al. 2002), to detect sites of kidney bleeding. *Postmortem* inspection of all abdominal organs did not detect injury to any other organs.

Cavitation detection system

A cavitation detection system was engineered and mounted on the bottom of the water tank, as shown in Fig. 1b. Two single-element focused transducers (diameter 10 cm, radius of curvature 10 cm, frequency 1.1 MHz) were mounted on a bracket affixed to the SW reflector and aligned confocally to sample a $5 \times 5 \times 5$ mm^3 volume (please see details below). The received signals were filtered by a 300-kHz high-pass filter (model 3202, Krohn-hite, Avon, MA, USA) and recorded on a Tektronix TDS 520 digitizer (Beaverton, OR, USA). Sampling frequency was 5 MHz and 1 ms of data were collected for each SW. A photodiode that detected the light output of the underwater spark triggered data collection from 24 successive SWs administered at 2 Hz.

A C15/4-2 SonoSite scan-head (Bothell, WA, USA) was mounted between the PCD transducers. The scan head frequency was 2–4 MHz. The scan head and US gel were placed in a thin plastic sleeve (ATL/Philips, Bothell, WA, USA) to protect the scan head, but also to ensure acoustic coupling with the water. A corprene hood protected the scan head from energy generated by the PCD transducers and the lithotripter.

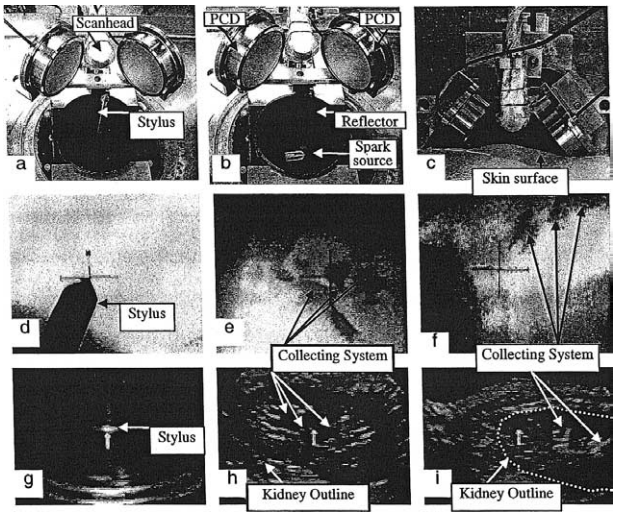

Fig. 1. Components and alignment of the cavitation detection system. (Top row) Detection system including PCD transducers and US scan head are shown mounted in lithotripter (a) with alignment stylus in place, (b) without stylus and (c) with pig in position. (center and bottom rows) Fluoroscopic and B-mode US images of alignment (*F2* indicated by cross-hairs and small arrow, respectively) (d), (g), on the stylus (e), (h), in the collecting system, and (f), (i) in the lower pole of the kidney. The X-ray images include the injection of contrast agent and were made after initial experiments in native urine to verify alignment, which, in all cases, was precise to within 2 mm.

The system was clamped to the lip of the lithotripter reflector (Fig. 1a b). It could rotate along that lip to optimize acoustic access to the pig kidney and simultaneously remain confocal with the lithotripter. We affixed the system in a position of about 8:30, considering the pig's head to be 12:00. The height of the detector was adjustable and the device could slide toward or away from the reflector. Each PCD transducer could be rotated and raised. Micropositioners controlled fine movements of the system. The US scan head could be moved forward or backward on the center-line of the PCD transducers, to touch the skin surface for better imaging or to retract the probe away from the SW path of the lithotripter.

The transducers and mounting bracket prevented inflation of the imaging balloons, but the quality of the fluoroscopic imaging was sufficient to identify kidney landmarks and to target the focus of the lithotripter.

Transducer calibration

The PCD transducers, their calibration and operation have been described in a previous publication (Cleveland et al. 2000b). A calibration of 9.5 MPa/V relates the maximum voltage at the PCD transducer to the peak positive pressure of the shock wave at a distance 10 mm from the bubble center. The axial and transverse dimensions of the sensitive volume (full-width half-maximum) were measured by a −6-dB in pressure drop-off and were 13 mm by 2 mm.

The transducers were also calibrated as 1.1 MHz sine wave generators. The signal source was a Hewlett-Packard (now Agilent) 33120A function generator and an ENI AP400B amplifier (Bloomfield, NY, USA). An electrical matching network was made to match the impedance of the transducer to the 50 Ω output of the amplifier. An in-line RF wattmeter (model 21A, Sonic Concepts, Woodinville, WA, USA) measured the true electrical power delivered to the transducer.

Acoustic spatial-average intensities were measured two ways, absorptive force balance and calibrated hydrophone (Sonic Technologies reference shock wave hydrophone, Hatboro, PA, USA; 0.6-mm active area). Acoustic powers measured in the force balance were divided by the −6-dB cross-sectional area of the beam (0.031 cm^2) determined by the hydrophone mapping. Peak pressure p was measured by the hydrophone. Spatial-peak intensity I_{SP} was calculated according to $I_{SP} = \rho^2/2\rho c$, where $\rho = 1000$ kg/m^3 and $c = 1500$ m/s are the density and the sound speed of water. Spatial-peak intensity was converted to spatial-average intensity I_{SAL} using the beam profile predicted by O'Neil (1949) as described by Hill (1971): $I_{SAL} = I_{SP}/1.8$. *In situ* intensities were time-averaged to incorporate the duty cycle and derated by 0.3 dB/MHz/cm, and the tissue depth was determined by US image.

Dual PCD

Coleman et al. (1996), Zhong et al. (1997) and Cleveland et al. (2000b) have used passive cavitation detection in lithotripsy. The acoustic trace characteristic of cavitation is two spikes, one corresponding to nonlinear scattering from bubbles present when the lithotripter shock pulse passes through the focal point and a second, from emission when the bubble collapses. The term nonlinear acoustic scattering encompasses SW scattering as well as emission from bubbles. The model by Church (1989) suggests that, when driven by a lithotripter pulse, a bubble first collapses, then undergoes a "first bounce" (emitting a pressure pulse), after which the bubble undergoes a sustained expansion phase before collapsing again and, on second bounce, emitting a second pressure pulse. These predictions were confirmed by using the measured coincidence of pressure pulses with sonoluminescence to identify the moments of collapse (Coleman et al. 1992) and laser scattering to identify the expansion phase (Jochele et al. 1995). The Church (1989) model was then used to predict a monotonic increase in the time of collapse t_c between the spikes (as well as the amplitude of the pressure wave radiated in collapse) with increasing drive voltage (Coleman et al. 1992), which was subsequently confirmed *in vivo* and *in vitro* (Zhong et al. 1997; Pye and Dineley 1999; Cunningham et al. 2001). The interval t_C is, therefore, often used as a measure of the collapse intensity. As bubbles are driven harder, their growth and collapse cycle lengthens. A monotonic relationship between lithotripter charging voltage and t_C is a check that signals are, indeed, cavitation.

Dual PCD uses two nearly orthogonal PCD transducers and coincidence detection to localize cavitation events. The sensitive volume of one detector is long and thin, but the intersection of two equal but orthogonal sensitive volumes is a region bounded only by the width. Thus, signals, detected simultaneously by both detectors and of nearly equal amplitude, are those that originate from only this small $5 \times 5 \times 5$ mm^3 region of intersection.

PCD signals were analyzed as described by Cleveland et al. (2000b). The algorithm was written in LabVIEW (National Instruments, Austin, TX, USA). Signals were high-pass filtered at 600 kHz because of noise that was apparently introduced at 300 kHz by saturation of the Krohn-hite filter. Signals were then rectified and demodulated to remove the 1.1-MHz ringing of the transducer. Each PCD signal was normalized to the amplitude of the first detected signals, the result of nonlinear scattering of the spark-generated direct wave. This was to compensate for different attenuations through different tissue paths for the two PCD transducers. A cross-correlation was used to make the initial signals coincident. Initial spikes varied by 1–5 μs, again because of the different tissue paths. Local maxima were identified on each signal. Because of the ringing of our transducer, the larger of two maxima within 10 μs of each other was selected and the other neglected. The maxima on both signals were compared to identify maxima within 8 μs of each other (*i.e.,* considered coincident). Last, the amplitudes of coincident signals were compared. Only signals that were within a factor or two of each other were retained. The rationale was that one event within the −6-dB region of both transducers had to register signals on both transducers that differed by no more than two. Collapse time, t_C, between initial spike and the primary collapse was recorded, as was the amplitude of the highest PCD maximum. Records were kept of how many PCD traces detected cavitation. Traces are

displayed with the second PCD signal inverted for easier comparison.

System alignment

Mechanical pointers that fit over each PCD transducer were made to indicate the focus of the transducers and to guide alignment with the stylus used to mark *F2* of the lithotripter (see Fig. 1a). Fluoroscopy confirmed the pointers at *F2* (see Fig. 1d). The angle between the PCD transducers was 90°. The US scan head was placed in its mount between the PCD transducers. Water was then added to the tank. The PCD pointers were removed. The US scan head was then raised or lowered to align the image at the tip of the stylus used to indicate *F2* (see Fig. 1g). An arrow symbol was entered on the US screen to mark the position of *F2*. The lithotripter stylus was then removed. When both PCD transducers were run as high-intensity focused US (HIFU) sources, they created an X (roughly 7 mm along each slash) of cavitation bubbles visible in the water at *F2*.

In preliminary experiments, a needle hydrophone was positioned at the tip of the *F2* pointer along the center-line of the PCD transducers and then removed. Each transducer was run as a source and its position was finely adjusted to maximize the hydrophone signal. Scattering from the hydrophone could also be used to align the other PCD transducer. However, mechanical alignment proved to be as accurate as the hydrophone alignment.

After alignment of the detection system with the lithotripter, the pig was lowered into the tank. The pig was moved into position under US guidance (see Fig. 1c). The renal pelvis was targeted first (see Fig. 1h). Because the speed of sound in tissue is slightly higher than that in water, the cross-hairs on the US screen indicated a spot 2 mm beyond *F2* (*i.e.,* true *F2* was 2 mm closer on the image). Likewise, refraction due to the sound speed difference meant the PCD beams focused the same distance toward the imaging scan head. In both these estimations it was assumed that tissue was homogeneous and that all refraction occurred at a plane tissue-water interface. Therefore, in tissue, the focal volumes of the PCD transducers produced a V, not an X as in water, with geometrical *F2* of the lithotripter located at the point of the V. No correction was made for refraction of the lithotripter beam, because the lithotripter focal region was large ($\sim$1.5 cm by $>$ 6 cm) in water and Cleveland et al. (1998) did not measure a significant effect of refraction when recording lithotripsy pulses with an *in vivo* hydrophone.

Shock wave treatment

For the first animal, X-ray contrast agent (commercial agent containing (diatrizonate meglumine and diatrizonate sodium) was injected *via* the ureteral catheter and fluoroscopy was used to target the lithotripter on the collecting system. In the other pigs, alignment was guided by US and fluoroscopy without the use of contrast agent. Alignment was confirmed in these animals after 200–300 SWs by administering contrast agent (see Fig. 1e, f, h, i) and, in each case, the target location identified under fluoroscopy was within 2 mm of the target location determined using US guidance alone. The lithotripter and the cavitation detection system were always focused on the same position in space.

Physical localization of sites of SW treatment in the renal parenchyma

Sites of SW treatment targeted within the renal parenchyma were marked by using the PCD transducers as high-intensity focused US (HIFU) sources. The sources were run at 50% duty cycle at the frame rate of the US imager. This was so that scattering from the PCD sources only obscured half the US image. With proper phasing, the interference could be relegated to the fringes of the image. At low power (I_{SAL} = 30 W/cm^2), streaming in fluid was seen (Shi et al. 2001). At high power (I_{SAL} = 1200 W/cm^2), a bright spot could be seen on the US image within a few s (Vaezy et al. 2000). The high power was left on for 5–10 s and caused thermal coagulation of the tissue in a region roughly the size of the −6-dB pressure region. HIFU left a clearly observable lesion that marked the region that had been interrogated by B-mode US and dual PCD. Lesions were viewed in slices of the kidneys, which were each fixed and embedded in wax (Blomgren et al. 1997). In this way, we were able to confirm that tissue refraction did not disrupt the alignment of the PCD transducers and the US imager.

RESULTS

For each animal, the renal collecting system was targeted first. After assessment of cavitation in native urine or urine mixed with X-ray contrast agent, the animal was repositioned so that *F2* of the lithotripter was within the renal parenchyma and the cavitation detection system was interrogating tissue.

Collecting system

Echo indicative of cavitation was readily detected in the urine collecting system by B-mode US. Indeed, echo was visible within the first several SWs delivered. When SWs were administered at a clinical rate (0.5–3 Hz), we observed three phases in the appearance of echo. The reader is reminded that these phases are the distillation of our visual impression of B-mode images in a specific pig, not patient, model. During the first few SWs, the signal was faint and sporadic but increased in frequency of

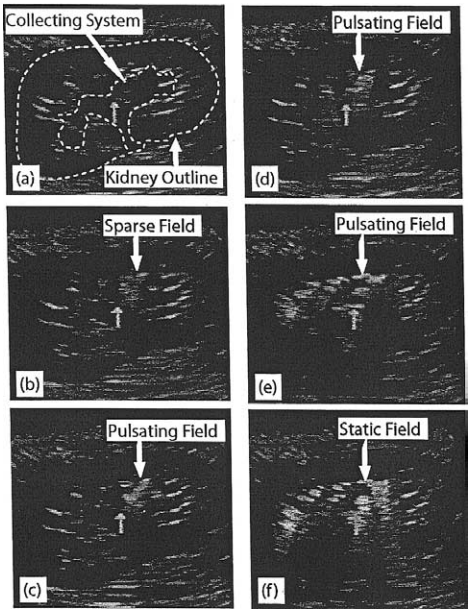

Fig. 2. Sequence of B-mode images showing stages of echogenicity in the urine collecting system of the kidney. A small white arrow marks *F2* of the lithotripter. (a) The collecting system (outlined by dashed line), prior to administration of SWs, is hypoechoic. (b) "Sparse field" appears faintly echogenic after several SWs and disappears. (c) "Pulsating field" is brighter and persists. (d) Pulsating field pulsates with each SW and, in this frame, shrinks and loses echogenicity compared with the previous SW in (c). (e) In general, the pulsating field grows and becomes brighter over a SW sequence. (f) "Static field" fills the collecting system and does not pulsate. Comet-tails (imaging artifacts) are seen (f) on the left and right and likely result from reverberations of the imaging pulse within a cloud of high-void fraction.

occurrence and longevity as treatment continued. Here we describe this phase as the "sparse field." After about 150–250 SWs, echoic clouds became brighter and persistent and pulsated with each lithotripter pulse. This "pulsating field" grew in intensity and size for another 20–200 SWs, until echo filled the collecting system on the image and the bright cloud ceased to pulse with each SW (*i.e.,* "static field"). Figure 2 shows selected video frames of the development of the echogenic region. When SWL was stopped, it took several minutes for echogenicity to dissipate. More intense echo took longer to dissipate, perhaps indicating larger bubbles. After a waiting period while bubbles dissipated, administration of SWs reproduced several times in each pig the same three-phase progression.

Dual PCD signals were readily detected in the collecting system during the "sparse field" and "pulsating field" phases, but not during the "static field" phase. Figure 3 shows a representative trace at 21 kV. PCD channel 1 is plotted above the $p = 0$ axis, and PCD channel 2 is inverted and plotted below the $p = 0$ axis. The initial spike at 60 μs is nonlinear scattering from existing bubbles. The amplitude of the initial spike tended to increase with echogenicity, and noise followed the spike, presumably caused by other bubbles collapsing and reverberation paths through tissue. The larger spike at 500 μs is the emission from bubble collapse. The characteristic time or collapse time t_C is the difference between the first and second peaks, 440 μs. Bubble rebound, the secondary growth and collapse phase of the bubble, is evidenced by a third slightly lower amplitude spike at 660 μs. The small signal at 25 μs is caused by scattering of the direct (unfocused) wave diverging from the lithotripter spark. Confirmation that a PCD signal is from cavitation can be obtained by looking for an increase in t_C at increasing charging potential of the lithotripter (Coleman et al. 1996). The t_C values collected in the "pulsating field" were 240, 340, 370, 400 and 500 μs $\pm$ 10% for charging potentials of 12, 15, 18, 21 and 24 kV, respectively. At one kV setting, t_C often grew to and then maintained a maximum value in 5–10 SWs. Absolute values varied depending on conditions and increased with higher SW number and brighter echogenicity. However, if coincident signals were measured, t_C always increased with increase in charging potential.

A plot of t_C values vs. SW number for the "sparse field" in the collecting system is shown in Fig. 4. Data are for the first 176 SWs delivered to native urine, without addition of X-ray contrast agent. Sporadic and increasingly extended bouts of cavitation signal were observed that correlated with the appearance of echo

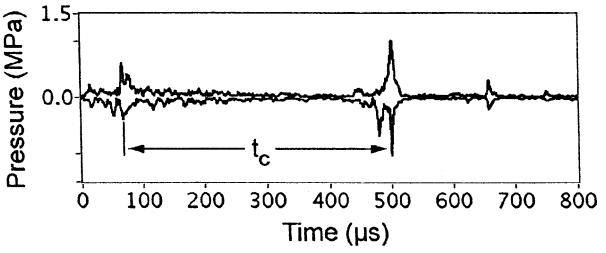

Fig. 3. Dual PCD trace, showing coincident cavitation signals in native urine at 21 kV charging potential. The second channel is inverted for coincident comparison. An initial spike at 25 μs occurs caused by the direct SW spherically diverging from the spark and nonlinearly scattering from bubbles at *F2*. At 60 μs, the first signal of the cavitation double-spike signal is seen, the result of nonlinear scattering of spark-generated SW focused by the reflector from bubbles at *F2*. Low-amplitude noise because of scattering in the tissue follows this signal. The collapse spike, detected coincidently on the upper and lower (inverted) trace, is at 500 μs: collapse time t_c is the difference, 440 μs. Collapse amplitude is 1 MPa. Coincident detection is able to distinguish the high-amplitude collapse in the focus of both transducers from other collapses detected in the focus of only one transducer. Note that PCD channel 2 detected a collapse just before the coincident signal, that was not detected by PCD channel 1. A rebound collapse of the cloud is seen at 660 μs.

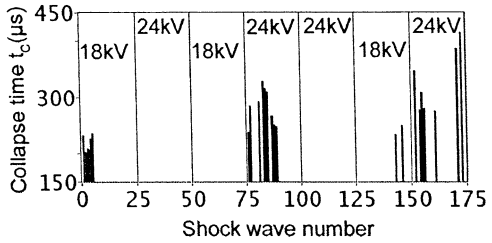

Fig. 4. Plot of t_c values during the "sparse field" phase of cavitation in native urine. PCD signals were detected from the first several SWs delivered to the pig and, then, cavitation was not detected again until after 75 SWs. Cavitation reappears, starting at SW #142. With increasing SW number, cavitation activity persists longer and occurs more frequently. The t_c values increase with kV setting and with SW number. Echo appeared on B-mode only when PCD signals were detected.

although, sometimes, echo was not perceptible. In both animals that did not receive contrast agent at the start, the first few SWs produced cavitation signals but, then, cavitation was inconsistent with subsequent pulses. This result suggests that there were preexisting cavitation nuclei in the urine and that these nuclei were eliminated or moved out of the acoustic field, possibly because of acoustic forces, as treatment proceeded. With continued SW treatment, the string of consecutive pulses that generated cavitation grew longer. Then, after about 150–250 SWs, there was persistent cavitation showing as pulsating intense echogenicity and a PCD signal with almost every pulse.

Echogenicity and PCD signals evolved during the course of treatment. Figure 5 shows the dual PCD data corresponding to the sparse, pulsating and static fields observed on B-mode before and after injection of X-ray contrast agent. The upper plot is peak PCD amplitude, and the lower plot is t_C. Both values are plotted against SW number. The sequence begins with a sparse field: amplitudes are moderate, collapse times are low and then coincident signals disappear. Cavitation signals last for the duration of the pulsating field, and t_C is long. When the cloud became static, cavitation signals stopped. Injection of X-ray contrast agent immediately increased t_C, amplitude and frequency of cavitation occurrence (seen in Fig. 5) and also intensified echo seen on the B-mode images. The inference is that the flowing contrast agent disrupted the cloud sufficiently to reinstate cavitation. The average t_C was 1.5 times greater with contrast agent than in native urine, 400 ± 60 μs vs. 240 ± 46 μs at 18kV and 572 ± 61 μs vs. 340 ± 57 μs at 24kV. In both media, t_C at 24 kV was 5/3 times the t_C at 18 kV. The t_C and amplitude increased during the "pulsating field" but, although t_C remained high, the amplitude diminished (SW #25 and 54) in the transition to the static field. Also, some SWs did not produce detected cavitation signals and some did, in the transition. Thus, the transition to "static field" occurred over the span of a few SWs. In another animal, the frequency of cavitation detection for six chronological 10-SW series identical to Fig. 5 were 60, 40, 10, 100, 100 and 80 %, where contrast agent was injected after the third step. Cavitation achieved "static field" during the 10% and 80% steps. Also, if SW treatment was halted after a "pulsating field" was achieved, this phase became re-established with only 10 SWs, even with a pause of several min in SW delivery.

With attainment of a "static field," the occurrence of PCD signals fell dramatically. So, although there was intense echo, arguably from bubbles, bubble collapses were not detected. Figure 6 shows a PCD trace (Fig. 6a) in the pulsating field and (Fig. 6b) in the static field five SWs later. In the static field, coincident collapse signals were very rare and amplitude of the initial spike was very large. The initial spike increased in the pulsating cloud also, but not to the same extent and, as might be expected, correlated with intense echo. Echogenic regions that extended a good distance toward a PCD transducer produced a slightly earlier arrival time of the initial signal, because of the shorted travel path of the scattered SW. We conclude that the void fraction was too high in the static field and that the SW nonlinearly scattered

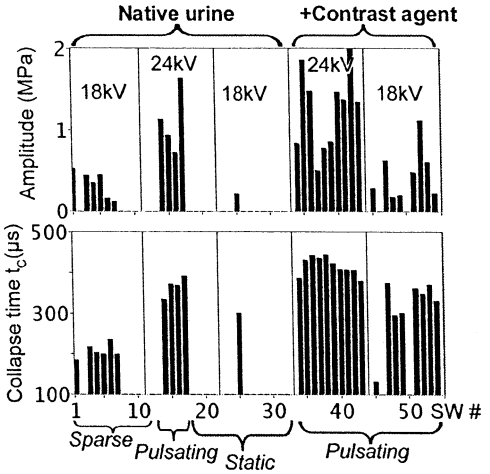

Fig. 5. Example of cavitation cloud evolution in SWL. PCD signal amplitude and t_c are plotted vs. SW number. X-ray contrast agent was injected after SW #30, as indicated on top. Echogenic field observed on simultaneous B-mode is described along the bottom. The sequence begins with a sparse field and frequent cavitation signals are detected. A pulsating sustained field of echogenicity follows with high-amplitude long-t_c PCD signals. When the cloud becomes static, cavitation signals cease. Contrast agent injection immediately increases t_c, amplitude and frequency of cavitation occurrence. Echogenicity of pulsating cloud also increased. Frequency decreases as the field moves to a static condition again, not shown. High t_c but low amplitude, as seen in SWs #25 and 54, was common for signals during transition to static field or for infrequent signals in static field.

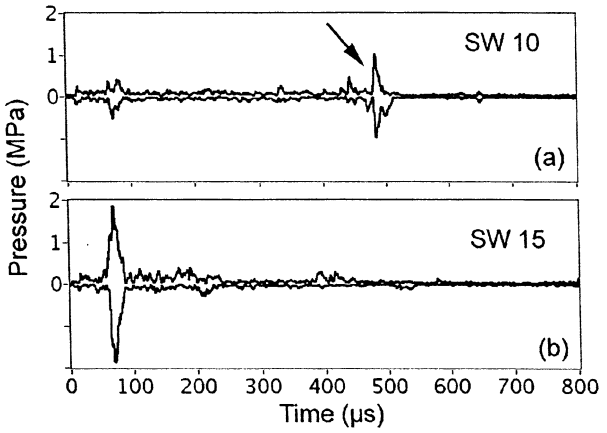

Fig. 6. PCD trace in (a) pulsating field and (b) static field. In the static field, coincident collapse signals are very rare and, instead, amplitude of the initial spike, produced by nonlinear scattering from the bubbles, is very large. It appears that the cloud is too densely populated or consists of sufficiently large bubbles so that sound is reflected or emitted but not concentrated into oscillation and collapse.

from the low impedance of the cloud interface, rather than penetrating the cloud to drive bubble oscillation and collapse.

As a rough quantitative check of this speculative conclusion, the following problem was posed: how many bubbles are required to attenuate the SW *en route* to the center of the collecting system? It was estimated that the negative pressure of the SW attenuates from −10 MPa to −1 MPa in 0.5 cm. For a peak negative pressure amplitude less than 1 MPa, the t_C predicted using the Church (1989), model is shorter than the ringing of our PCD and, therefore, irresolvable with our system. The attenuation distance was estimated from the kidney geometry. These estimates give an attenuation of 460 Np/m. We estimate bubbles were on the order of 10 μm. Church (1989), Sapozhnikov et al. (2002), and Tanguay and Colonius (2003) calculated that the equilibrium radius of the bubble is 30 μm following collapse and then the bubble partially dissolves before the next SW. Tanguay and Colonius (2003) have shown that the equilibrium bubble radius asymptotes for a given SW delivery rate, if bubble agglomeration and fission are neglected. The fundamental frequency of the lithotripter pulse, which is 4 μs in duration, is 250 kHz (Cleveland et al. 2000a, Coleman et al. 1989). With this attenuation, frequency and bubble radius, the dispersion relation defined by Foldy (1945) was used to predict a void fraction (ratio of volume of gas to volume of the bubbly mixture) of approximately 10^{-5}, or 2400 bubbles/cm. If these bubbles were to grow to a maximum radius of 0.5 mm (predicted for water by (Church 1989), a void fraction of 1 would be obtained, which means the whole region is gas and this is a logical upper bound. Studies (Sapozhnikov et al. 2002, Tanguay and Colonius 2003) show that the bubbles do not grow as large when the number density is high, but other studies (Pishchalnikov et al. 2003) show agglomeration of bubbles is possible. Therefore, these rough estimates support the speculative conclusion that the bubble cloud can dramatically attenuate the SW below a threshold level to produce detectable cavitation.

Kidney parenchyma

Cavitation was detected in the kidney parenchyma, both as echo and coincident PCD signals. Whereas, in the urine collecting system, cavitation signals were detected from the very beginning of SW exposure, it required approximately 1000 SWs to initiate cavitation in tissue. Figure 7 shows the onset of echogenicity within tissue. A dashed line outlines the kidney in each image. The kidney center, the collecting system, appears hy-

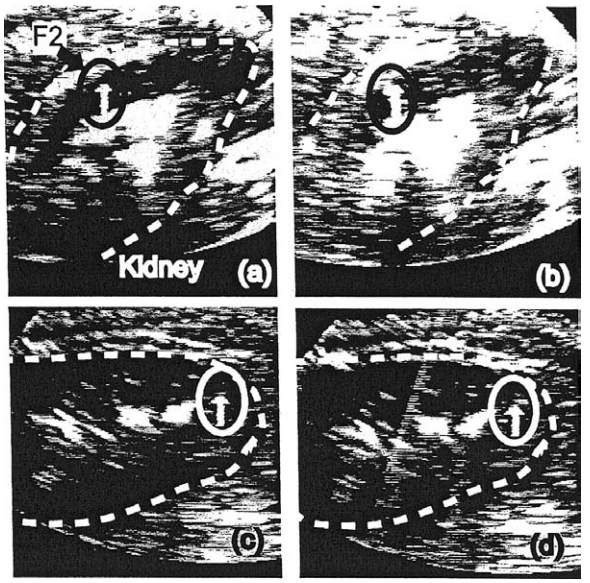

Fig. 7. Shock-wave-induced echogenicity in kidney tissue. B-mode images show (a), (c) lack of echogenicity before SWs and (b), (d) sudden appearance of echogenicity within the tissue parenchyma as SWs are delivered. Two tissue sites are shown: (above) corticomedullary junction of middle pole and (below) lower pole. (----) Kidney outline around the lower pole. The collecting system in center of the kidney is echogenic in all images; tissue image is generally dark. Ring around white arrow points to the interrogated region centered at *F2*. (b) Echo appears along the length of the arrow and appears to connect the echogenicity in the collecting system with that in a growing echogenic subcapusular hematoma (hematoma confirmed *post mortem*) on top of the kidney as imaged. (d) Echogenicity surrounded by hypoechogenic tissue. Appearance correlated to within one SW of the first appearance of PCD coincident signals at these locations in the tissue.

perechoic, which is the result of many applied SWs. The arrow on the US image, ringed in black or white on the image, indicates the region of interrogation at *F2*. On the left in Fig 7a, negligible echo is observed around the arrow in the corticomedullary junction of the middle pole; on the right in Fig. 7b, hyperecho runs the length of the arrow and appears to bridge echo in the collecting system and in a growing subcapsular hematoma (the result of earlier treatment of the lower pole). The bridge was seen on the US image to form over three to six SWs after several hundred SWs and then remained. Both the subcapular hematoma and a hemorrhagic lesion bridging the hematoma and the collecting system are observed in the *postmortem* section (Fig. 8) of this kidney. In Fig. 7c, the lower pole of another kidney is not echogenic and then, in Fig. 7d, an echogenic region appears surrounded by tissue. After echo started in tissue, it persisted, grew brighter, grew slightly in area and, like cavitation in the collecting system, pulsated with each SW.

Dual PCD signals were detected concurrently and colocated with the echo. Figure 9 shows a PCD trace from the parenchyma of the middle pole of the kidney, the same cavitation cluster and location shown in Fig. 7b. The initial spike amplitude was large and increased when echo and collapse signal were observed. The collapse signal is at 450 μs, which yields a t_C of 385 μs. The t_C values increased with kV and with SW number as brightness increased. Measured t_C values in tissue were 280 $\pm$ 30 μs and 390 $\pm$ 60 μs at 18 and 24 kV, which was comparable with the t_C measured in native urine in the collecting system. Dual PCD makes it possible to reject the small cavitation signal at 440 μs, because it appears on channel 2 only. Thus, both dual PCD and B-mode US gave simultaneous indication of cavitation within tissue during SWL.

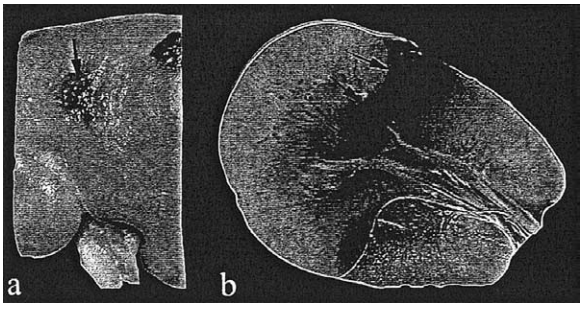

Fig. 8. SWL-induced hemorrhagic tissue injury in kidney viewed by US in Fig. 7a, b. (a) Subcapsular hematoma, seen as a subcapsular echogenic region in Fig. 7a and b, on the kidney surface (arrow). (b) Hemorrhagic region from capsule to collecting system (arrows) corresponds to location of the echogenic bridge in Fig. 7b. Note that Fig. 8 is a coronal cross-section and that Fig. 7b is a sagital cross-section, but both are from the center of the kidney.

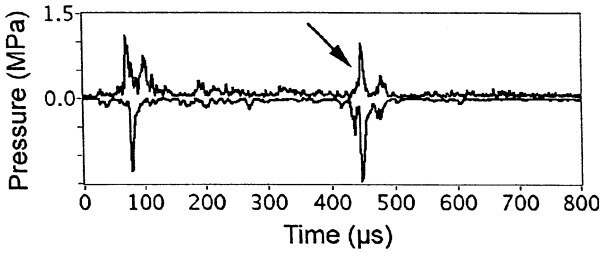

Fig. 9. PCD signal detected in kidney parenchyma during SWL. Kidney had received over 1000 SWs, half at 18 kV and half at 24 kV. PCD signals correlated with spatial and temporal appearance of echogenicity in Fig. 7b. Amplitude and t_c are similar to data in native urine (*e.g.,* see Fig. 3).

Although tissue might be expected to restrict bubble growth and to shorten t_C (Ding and Gracewski 1994), the limited evidence is not consistent. Zhong et al. (1997) using PCD in SWL *in vivo,* recorded t_C values shorter than those in water; however, Coleman et al. (1999), using PCD in patients, recorded t_C values equal to those in water. Neither could be sure to separate tissue from liquid space. Church (2003) discusses many factors that can complicate the expansion of a bubble in tissue near other bubbles. Our evidence above indicates that t_C is very sensitive to SW rate, history and the fluid medium. But long t_C correlated with strong echogenicity. Therefore, we believe that the dominant factor on t_C was not tissue constraint but bubble number density, as discussed further in the Discussion section.

Confirmation of alignment in tissue

After cavitation detection during SW administration, tissue sites of detection were marked by using the PCD transducers as HIFU sources thermally to necrose the interrogated region. The location of the thermal lesion agreed with the location of cavitation detection predicted by US and fluoroscopic imaging. Figure 10a shows a slice of a kidney that was treated with SWs, interrogated for cavitation and marked with a thermal lesion. There is a clear thermal lesion that resulted from the HIFU. The damage is most concentrated deepest in the tissue and then grows more diffuse toward the capsule. Previous research (*e.g.,* Watkin et al. 1997) indicates that lower amplitudes or shorter exposures would prevent this growth to the capsule and create an even more localized marker. The white necrotic HIFU lesion is distinct from the hemorrhagic SWL-induced injury (Watkin et al. 1997; Evan et al. 1998), but SWL injury was not quantified in this kidney. The injury in Fig. 10a is in the lower pole and its position agrees well with the position indicated in Fig. 7d. Cavitation detection in the parenchyma was, in fact, in the parenchyma and refraction played no role other than that predicted in distorting the location of the interrogation region.

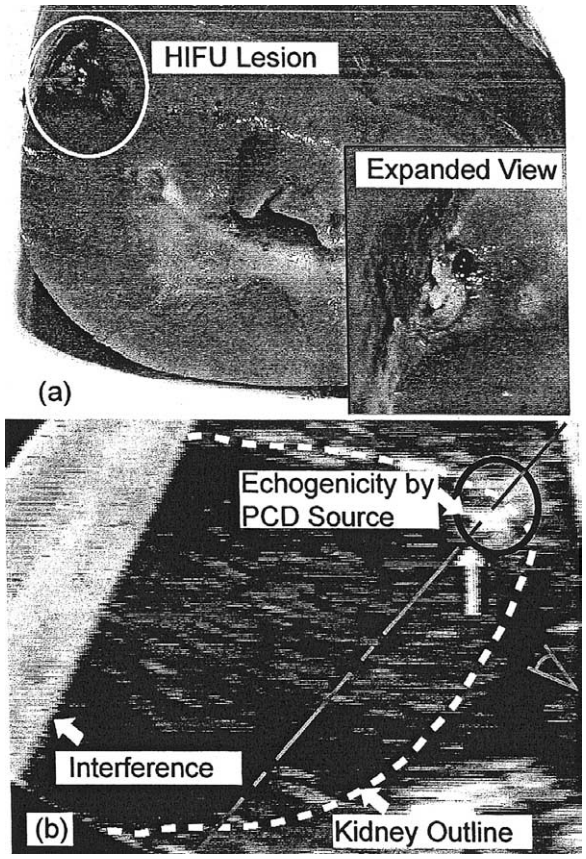

Fig. 10. Verification of site of cavitation detection within kidney tissue by HIFU-induced necrosis and echogenicity. (a) HIFU lesion created to mark the detection region of PCD transducers. Detection was in tissue and confirms the location of cavitation detection indicated in Fig. 7d. Expanded view shows that the thermal lesion created by HIFU is distinct from SWL-induced injury, as shown in Fig. 8. (b) While HIFU (PCD transducer on the right in this case) is on, an echoic region is observed in the focal region and offers yet another indicator of alignment in tissue. The echogenic region began within the tissue and grew to the kidney capsule. (----) Coronal cut that was taken for the section in (a); blue eye indicates the viewing angle in (a).

One final method of confirming the location was that the HIFU sources produced echogenic regions on B-mode US. Hence, by insonifying the tissue with the PCD transducers run as HIFU sources and simultaneously imaging with B-mode, it was possible to observe and locate the focal interrogation region of the PCD transducers in tissue in real time. The echogenic region shown in Fig. 10b was produced by exciting only the PCD transducer on the right and is exactly at the predicted interrogation region indicated by the arrow. The echogenic region location agrees with the lesion location in Fig. 10a. The size and shape of the echogenic region correlates with the dimensions of the thermally necrosed region (see Fig. 10a) that has been shown before in HIFU studies in liver (Vaezy et al. 2000). In addition, following the results published by Vaezy and colleagues, it was seen that, if the HIFU source was turned off as soon as the echogenic region appeared, no gross thermal lesion was observed. Last, when the PCD transducer was focused in fluid (urine space or hematoma) and run as a source, even at low intensity (I_{SPTA} less than 30 W/cm^2), a faint echo on the B-mode showed flow in the focus moving away from the transducer. Thus, it was readily confirmed at low intensity without tissue injury when the PCD was focused in fluid space, as opposed to tissue.

DISCUSSION AND SUMMARY

The research reported here is significant for four reasons. First and foremost, cavitation was detected in the renal parenchyma during lithotripsy, because this study design was able to pinpoint the precise localization of cavitation within kidney tissue. Second, it was observed, in a specific pig model, that the bubble cloud in the collecting system evolves to a point where SWs appear to be reflected by the cloud and bubble collapse was not detected. Third, the detection system lays the framework for a feedback system that may help urologists to identify highly reflective static clouds that may shield renal calculi from comminuting SWs. Fourth, the documented change in cavitation behavior with ureteral injection of X-ray contrast agent, which is not uncommon in patients in the HM3, raises the potential to infuse the collecting space with an appropriate cavitation-promoting or -mitigating agent to improve comminution. These points are discussed below, with the first point discussed last.

Cavitation was observed in pigs by B-mode US and dual passive cavitation detection (PCD), both within the fluid-filled space of the urine-collecting system and within the renal parenchyma, during SWL. There was excellent temporal and spatial correlation between echogenicity and coincident dual PCD signals. Cavitation in the urine occurred readily, but detection of bubble activity in tissue required continuous treatment with hundreds of SWs.

B-mode US gave visual orientation to the kidney and provided visual evidence of bubble activity that was critical to interpretation of the dual PCD traces. The pattern and intensity of echogenicity depended upon the area of the kidney being targeted (*i.e.,* collecting system vs. tissue) and/or the number of SWs delivered. Our qualitative description of three stages in the development of cavitation is not intended to be a thorough characterization of bubble activity in the kidney but, instead, is presented as a frame of reference for our interpretation that cavitation in this specific pig model was, indeed, detected in the urine space and in kidney tissue. Cavita-

tion was progressive, weak at first and increasing with successive SWs. The pattern was easier to see in the urine space, but could be observed in tissue as well.

The ease with which cavitation was observed in the collecting system is important to SWL. One might assume that there are fewer cavitation nuclei *in vivo* than *in vitro,* because of intense filtering by the lungs. Indeed, even *in vitro,* fewer cavitation-induced pits resulted in aluminum foil in urine than in foil in tap water (Lifshitz et al. 1997). However, in the current study, the very first SWs delivered to the collecting system produced echo and cavitation signals, which indicates that bubble nuclei were already present in native urine *in vivo.* Echo was faint and PCD signals faded but returned intermittently in this initial stage, indicating, perhaps, few nuclei and bubbles that drifted or were forced out of the target zone. Sometimes, PCD signals were detected without being able to discem echo. The collapse times of bubble clouds in the "sparse field" phase were rather short, but amplitudes of the collapse emissions were moderate to high. We speculate that bubble-bubble interactions were low and that bubbles collapsed spherically, with limited loss of collapse energy through fluid-jet flow. These experiments were conducted in animals that did not have kidney stones. One might speculate, as has been shown *in vitro* (Pishchalnikov et al. 2003), that the presence of a stone at the lithotripter focus would nucleate even more bubbles, which, in sufficient numbers, collapse asymmetrically as a cluster. The current observations suggest that the undisturbed (*i.e.,* no added X-ray contrast agent) environment of the collecting system immediately yielded cavitating bubbles and that the number of bubbles increased over the course of treatment.

With continued administration of ~200 SWs, the initial "sparse field" of bubble clouds developed into a brighter sustained "pulsating field", in which the cloud appeared to grow in size and bubble density. Brightness, t_c, and frequency of cavitation occurrence increase together, but amplitude after an initial increase decreases with brightness toward the end of the pulsating field, ~50 SWs later. Bubble cloud simulations (Tanguay and Colonius 2003) and high-speed movies (Sapozhnikov et al. 2002) have indicated that more densely populated clouds have longer t_c and smaller bubbles. High void fractions can lead to lower collapse energy in the simulated cloud collapse. Weaker collapse could be responsible, along with acoustic shielding of the stone by the cloud, for lower comminution at higher SW-delivery rates (Paterson et al. 2002; Pace et al. 2003). Physically, we might attribute the weakened collapse to increased compressibility of the fluid/bubble mixture that, through attenuation and bubble compression, reduces the pressure felt by bubbles in the cloud interior.

The pulsating clouds became more echoic, with longer t_c and a higher frequency of PCD signals following injection of X-ray contrast agent. An X-ray contrast agent is used at some clinical centers to aid in stone localization and targeting, but not with the goal of influencing cavitation. This result shows that cavitation can be altered by introduction of medium through a ureteral catheter. One may speculate that addition of the right medium could be used either to enhance or to mitigate cavitation, with the goal of improving stone comminution.

We observed that the bubble cloud eventually saturated the collecting system. The "pulsating field" gave way to a static cloud (*i.e.,* "static field"), densely populated with intense echo that filled the urine space. At this point, the PCD detected a high-amplitude first signal, but no delayed collapse signal. It appeared that there was no observable growth and collapse of bubbles and that the initial signal was very high amplitude. We speculate on two possible processes here. In one process, the bubbles on the periphery or in the cloud collapse with the impact of the lithotripter SW. As has been predicted in clouds, the collapse of outer bubbles reinforces the collapse of inner bubbles, creating a high-amplitude collapse signal. The asymmetrical and sequential initial collapse of these bubbles in the cloud prevents them from growing, collapsing and yielding a detectable acoustic emission (or, we speculate, a damaging impact on a stone). The second process provides a more satisfying explanation to us. The SW appeared to reflect from, not to penetrate, the cloud. Such a cloud presents a barrier to SWs and would presumably shield a stone from comminution. The amplitude of SW reflection was higher than that of even the largest collapse signals, a condition suggestive of the large impedance mismatch that would be expected for a water-gas interface. This interface was likely larger than a single scattering bubble, which helps to explain the high amplitude, because a plane reflection does not suffer the spherically-diverging losses that the collapse signal suffers. Also, the bubble collapse generates a SW of shorter duration (*i.e.,* more energy in higher frequencies) than the lithotripter SW. US attenuation in tissue generally increases with frequency, which leads to the emitted collapse signal being more attenuated and, in addition, the narrow-band PCD transducers are not sensitive to frequencies above 2 MHz (Coleman et al. 1996). In summary, distinct phases of cavitation activity were observed which, we speculate, may produce different stone comminution and tissue injury.

The detection system that we have described is a prototype research tool, but provides a method to monitor and qualitatively to characterize cavitation. A B-mode imaging system synchronized with SW delivery could improve sensitivity, because *F2* could be interro-

gated immediately following SW arrival. Currently, we are only detecting residual bubbles remaining after cavitation collapse on B-mode, which act as nuclei for the next SW (Sapozhnikov et al. 2002). However, with a synchronized active cavitation system, it might be possible to monitor bubbles during growth and collapse. It seems reasonable to suggest that observation of attainment of a "static field" of cavitation could be used as a clue to reduce the rate of SW delivery or, pause treatment. The potential also exists for a feedback system on cavitation in tissue and, possibly, tissue injury.

The key finding from this study is that cavitation can occur in the kidney parenchyma during SWL. That is, cavitation occurs not only within the urine collecting system but also within kidney tissue. B-mode US and dual passive cavitation detection simultaneously recorded evidence of cavitation in the kidney parenchyma, and PCD signals were responsive to changes in lithotripter kV. Spatial resolution of the detection system could easily differentiate urine space from the surrounding tissue.

This study was not designed to determine the threshold for production of cavitation in kidney tissue. Instead, SWs were delivered first to the collecting system. From our previous experience, we know that SW exposure stimulates a vasoconstrictive response in the kidney that affects injury caused by subsequent treatment (Willis et al. 2004). Thus, in the current study, the delivery of SWs to the collecting system may very well have influenced the ability of the surrounding tissue to support cavitation. With this in mind, we can describe that cavitation occurred readily in the urine space, but required a considerable dose of continuous pulses (about 1000 SWs in each animal) to develop in tissue.

Although not designed to correlate cavitation spatially or temporally with tissue injury, this study lays the foundation for future investigation. A most interesting question about SWL tissue injury is, "What initiates injury?" SWL-induced injury, termed "lithotripsy nephritis," is a vascular injury, with the smallest vessels rupturing first (Evan et al. 1998). Likely, this injury begins slowly and grows. Isolated vessel ruptures or cavitation events may initially be difficult to find. Three processes have been proposed for this initial injury. These are vessel puncture caused by cavitation collapse, vessel rupture caused by bubble expansion (Carstensen et al. 1990; Zhong et al. 2001) or vessel tearing because of pressure gradients in the SW (Lokhandwalla and Sturtevant 2000). This report lays some of the groundwork for distinguishing among these mechanisms. Vessel breaks lead to blood pooling and cavitation in the pooled blood, which, we speculate, then becomes the dominant mechanism of injury. Other evidence links cavitation, although not yet proven to initiate injury, with observed injury (Delius et al. 1989; Evan et al. 2002). It is interesting to note that a sustained pulsating cavitation cloud was observed in the collecting system after 150–250 SWs, which is comparable with published times for the observation of hematuria (Evan et al. 1998) and, in tissue, after 1000 SWs, which is comparable with the threshold number for observed tissue injury (Evan et al. 1998). In addition, the first observed cavitation is in the collecting system, which is bounded by the renal papillae, which are the first sites of injury.

CONCLUSION

A detection system, in which dual passive receivers and B-mode US were coaligned with the focal point of a Dornier HM3 lithotripter, was used to demonstrate that cavitation can occur in renal tissue, as well as in the urine collecting system, during SW treatment. Cavitation in the kidney was progressive and increased as more SWs were delivered. Bubble dynamics in the urine space suggest that acoustic shielding may develop during continuous SW delivery. The current study does not address the mechanisms of tissue damage in SWL, but provides direct evidence that cavitation occurs in the renal parenchyma during shock-wave lithotripsy.

ACKNOWLEDGEMENTS

The authors thank the many members of the Consortium on Shock Waves in Medicine for discussions, research help and guidance on this paper. Many complicated preliminary experiments went into this paper and they benefited from technical help from making the devices through interpreting the images to the animal protocol. In particular, the authors thank Philip Blomgren (Indiana University School of Medicine) for histological analysis and the research staff at Clarian Methodist Hospital in Indianapolis for their help and cooperation. They also acknowledge guidance on clinical SWL by Dr. James Lingeman at Methodist Hospital Institute for Kidney Stone Disease and Indiana University School of Medicine. The authors are also grateful for the detailed and thoughtful comments of the referees, which improved the clarity of the presentation as well as leading to additional calculations to test their speculative conclusions. The work was supported primarily by NIH (grants DK43881 and DK55674), with help from NSBRI (grant SMS00203), an NIH Fogarty International Research Collaboration Award, an ONR International Field Office Visiting Scientist grant and a CRDF grant.

REFERENCES

Blomgren P, Connors BA, Lingeman JE, Willis L, Evan AP. Quantitation of shock wave lithotripsy-induced lesion in small and large pig kidneys. Anat Rec 1997;249(3):341–348.

Carstensen EL, Campbell DS, Hoffman D, Child SZ, Bellagarda EJ. Killing of *Drosophila* larvae by the fields of an electrohydraulic lithotripter. Ultrasound Med Biol 1990;16:687–698.

Church CC. A theoretical study of cavitation generated by an extracorporeal shock wave lithotripter. J Acoust Soc Am 1989;86:215–227.

Church CC. A theoretical study of acoustic cavitation produced by "positive-only" and "negative-only" pressure waves in relation to *in vivo* studies. Ultrasound Med Biol 2003;29(2):319–330.

Cleveland RO, Lifshitz DA, Connors BA, et al. *In vivo* pressure measurement of lithotripsy shock waves. Ultrasound Med Biol 1998;24:293–306.

Cleveland RO, Sapozhnikov OA, Bailey MR, Crum LA. A dual passive cavitation detector for localized detection of lithotripsy-induced cavitation *in vitro.* J Acoust Soc Am 2000b;107:1745–1758.

Cleveland RO, Bailey MR, Fineberg N, et al. Design and characterization of a research electrohydraulic lithotripter patterned after the Dornier HM3. Rev Scient Instrum 2000a;71(6):2514–2525.

Coleman AJ, Choi MJ, Saunders JE. Detection of acoustic emission from cavitation in tissue during extracorporeal lithotripsy. Ultrasound Med Biol 1996;22:1079–1087.

Coleman AJ, Choi MJ, Saunders JE, Leighton TG. Acoustic emission and sonoluminescence due to cavitation at the beam focus of an extracorporeal shock wave lithotripter. Ultrasound Med Biol 1992; 18:267–281.

Coleman AJ, Saunders JE, Choi MJ. An experimental shock wave generator for lithotripsy studies. Phys Med Biol 1989;34(11):1733–1742.

Coleman AJ, Verma PK, Cahill MD. Clinical evaluation of the cavitation threshold in patients undergoing lithotripsy. J Acoust Soc Am 1999;105(2 Part 2):1267.

Cunningham KB, Coleman A, Leighton TG, White PR. Characterising in vivo cavitation during lithotripsy with time-frequency methods. Acous Bull 2001;26(5):10–16.

Delius M, Mueller W, Goetz A, Liebich H-G, Brendel W. Biological effects of shock waves: Kidney hemorrhage in dogs at a fast shock wave administration rate of fifteen hertz. J Lithotripsy Stone Dis 1990;2(2):103–110.

Delius M, Gambihler S. Sonographic imaging of extracorporeal shock wave effects in the liver and gallbladder of dogs. Digestion 1992; 52:55–60.

Ding Z, Gracewski SM. Response of constrained and unconstrained bubbles to lithotripter shock wave pulses. J Acoust Soc Am 1994; 96:3636–3644.

Evan AP, Willis LR, Connors BA, et al. Kidney damage and renal functional changes are minimized by waveform control that suppresses cavitation in SWL. J Urol 2002;168(4 Part 1):1556–1562.

Evan AP, Willis LR, Lingeman J, McAteer JA. Renal trauma and the risk of long-term complications in shock wave lithotripsy. Nephron 1998;78:1–8.

Foldy LL. The multiple scattering of wave. Phys Rev 1945;67:107–119.

Hill CR. Ultrasonic exposure thresholds for changes in cells and tissues. J Acoust Soc Am 1971;52:667–672.

Jochele K, Debus J, Lorenz WJ, Huber PA. A new method of quantitative cavitation assessment in the field of a lithotripter. Ultrasound Med Biol 1995;22(8):1079–1087.

Kuwahara M, Loritani N, Kambe K, et al. Hyper-echoic region induced by focused shock waves *in vitro* and *in vivo:* Possibility of acoustic cavitation bubbles. J Lithotripsy Stone Dis 1989;1:282–288.

Lifshitz DA, Williams JC, Sturtevant B, et al. Quantitation of shock wave cavitation damage *in vitro.* Ultrasound Med Biol 1997;23(3): 461–471.

Lokhandwalla M, Sturtevant B. Fracture mechanics model of stone comminution in ESWL and implications for tissue damage, Phys Med Biol 2000;45(7):1923–1940.

O'Neil HT. Theory of focusing radiators. J Acoust Soc Am 1949;21: 516–526.

Pace KT, Harju M, Dyer S, et al. Shock wave lithotripsy at 60 or 120 shocks per minute: A randomized, single-blinded trial. J Urol 2003;169(4, Suppl.):487(A).

Paterson RF, Lifshitz DA, Lingeman JE, et al. Stone fragmentation during shock wave lithotripsy is improved by slowing the shock wave rate: Studies with a new animal model. J Urol 2002;168: 2211–2215.

Pishchalnikov YA, Sapozhnikov OA, Williams JC, Jr. et al. Cavitation bubble cluster activity in the breakage of kidney stones by lithotripter shock waves. J Endouro 2003;17(7):435–446.

Pye SD, Dineley JA. Characterisation of cavitational activity in lithotripter fields using a robust electromagnetic probe. Ultrasound Med Biol 1999;25(3):451–471.

Sapozhnikov OA, Khokhlova VA, Bailey MR, et al, Effect of overpressure and pulse repetition frequency on shock wave lithotripsy. J Acoust Soc Am 2002;112(3):1183–1195.

Shi X, Martin RW, Vaezy S, Kaczkowski P, Crum LA. Color Doppler detection of acoustic streaming in a hematoma model. Ultrasound Med Biol 2001;27(9):1255–1264.

Tanguay M, Colonius T. Progress in modeling and simulation of shock wave lithotripsy (SWL). Fifth International symposium on Cavitation (CAV2003), Osaka, Japan, 2003. http://iridium.me.es.osaka-u.ac.ip/cav2003/index1.html: paper OS-2-1-010.

Vaezy S, Shi X, Martin RW, et al. Real-time visualization of focused ultrasound therapy. Ultrasound Med Biol 2000;27:33–42.

Watkin WN, Morris SB, Rivens IH, ter Haar GR. High-intensity focused ultrasound ablation of the kidney in a large animal model. J Endourol 1997;11(3):191–196.

Willis LR, Evan AP, Connors BA, et al. Same-pole application of low- and high-energy shock waves protects kidney from SWL-induced tissue injury (Abstr.). J Urol 2004;171(4, Suppl. S):294.

Zhong P, Cioanta I, Cocks FH, Preminger GM. Inertial cavitation and associated acoustic emission produced during electrohydraulic shock wave lithotripsy. J Acoust Soc Am 1997;101(5, Part 1): 2940–2950.

Zhong P, Zhou Y, Zhu S. Dynamics of bubble oscillation in constrained media and mechanisms of vessel rupture in SWL. Ultrasound Med Biol 2001;27:119–134.

Zhu S, Dreyer T, Liebler M, et al. Reduction of tissue injury in shock-wave lithotripsy by using an acoustic diode. Ultrasound Med Biol 2004;30(5):675–682.